Transitions in filament geometry drive ESCRT-III-mediated membrane remodelling and fission

Lena Harker-Kirschneck,[1,2] Buzz Baum,[2,3⋆*] Andela Šarić[1,2⋆*]

[1]Department of Physics & Astronomy, University College London, London, United Kingdom,
[2]Institute for the Physics of Living Systems, University College London, London, United Kingdom,
[3]MRC Laboratory for Molecular Cell Biology, University College London, London, United Kingdom

⋆ These authors contributed equally. *E-mail: b.baum@ucl.ac.uk, a.saric@ucl.ac.uk

ESCRT-III is an evolutionarily conserved membrane remodeling machinery that, with the Vps4 ATPase, forms filaments able to cut biological membranes from the cytosolic side. This activity of ESCRT-III is essential for the final stage of cell division in archaea and in many eukaryotes, the formation of vesicles, the creation of exosomes, the release of viruses such as HIV-1 and Ebola, and for the repair and sealing of cellular membranes. While there has been recent rapid progress in describing the biochemical and cell biology details of different ESCRT-III functions, we lack an understanding of the physical mechanism involved in ESCRT-III-mediated membrane remodelling. Here, through the development of coarse-grained molecular dynamic simulations, we present a minimal model that captures the ability of ESCRT-III to induce experimentally reported cases of ESCRT-III driven membrane sculpting, including the formation of cones and tubules, and membrane scission. This model

suggests a universal physical mechanism of action, that differs from that of other cytoskeletal elements, whereby a change in the twist of membrane bound ESCRT-III filaments drives transitions between a flat spiral and a 3D helix to induce membrane deformation and scission. We expect the mechanistic principles revealed here to be useful in manipulating ESCRT-III-driven processes in cells and in guiding the engineering of synthetic membrane-sculpting systems.

Cellular membranes require constant remodelling to allow cells to maintain homeostasis, to grow and to divide. This involves protein machines that can physically sculpt membranes in both directions, toward and away from the cytoplasm. The ESCRTIII family of proteins (endosomal sorting complexes required for transport III) is the only cellular apparatus known to deform and cut cell membranes protruding away from the cytoplasm. They do so by forming spiral/helical filaments that associate with the cytoplasmic face of biological membranes (*1–4*). This enables them to perform a wide range of membrane sculpting and snipping processes from archaeal to eukaryotic cells, such as cytokinesis (*5, 6*), multi-vesicular body formation (*7–9*), virus release (*10,11*), membrane repair (*12*), and nuclear envelope re-sealing (*13*). Despite many attempts to use physical principles to explain how ESCRTIII performs these functions (*14–17*) it is not clear how a single protein machine has the versatility to carry out this full range of functions.

While a recent model of ESCRT-III filaments as spiral springs (*18*) offers a simple way to link ESCRT-III polymer formation to membrane deformation, it is unable to explain: *i)* the sign of the deformation - spiral tension can be released in both upwards and downwards directions; *ii)* membrane scission, *iii)* the role of the Vps4 ATPase in ESCRT-III function, and *iv)* the ability of ESCRT-III to deform both flat and curved membranes.

Here, we have used molecular dynamics simulations to develop a new physical model of ESCRT-III filament function. Strikingly, our model suggests that a single filament geometry cannot explain the experimentally observed behaviours and that membrane shaping and topological transitions require energy-dependent transitions in chiral filament geometry.

Our nanoscale ESCRT-III filament model is built of beads connected by springs. The minimal unit required to construct a chiral filament that preserves its flat spiral shape was found to be a triplet of beads, where the beads of neighbouring triplets are interconnected (Fig. 1a, SI). Filament geometry is controlled by bond lengths linking neighbouring triplets (Fig. 1a), while rigidity, measured by filament persistence, is controlled by bond strength between the triplets. Since building units and bond lengths between neighbouring units are equal, the target geometry of such a filament is a closed ring of radius R. Though some ESCRT-III filaments are observed as rings (*1, 18–20*), the effects of volume-exclusion will force longer filaments to form spirals with the adoption of non-preferred curvatures causing a build-up of tension in the filament. Finally, the membrane-binding face of the filament is modelled as an interaction between two beads of the triplet (coloured in blue) and the membrane.

For simulations, pre-assembled planar ESCRT-III spirals (Fig. 1b) were placed on an equilibrated flat membrane, and followed over time as tension in the system was allowed to relax (Fig. 1c). Spirals attempt to reach mechanical equilibrium by contracting their outer and expanding their inner filament arms, as previously suggested (*18*). This leads to the formation of dense spirals, since the filament cannot overlap with itself. If the modelled filament was allowed to overlap with itself, it took on a resting ring shape. Remarkably, for any tested spiral geometry or level of stored tension, spirals remained effectively flat on the membrane (Video1), even when all the three beads of the filament triplets were allowed to bind to the membrane. Thus, under our model, a tense filament containing only in-membrane-plane curvature is not sufficient to drive membrane deformation. In line with this, *in-vitro* experiments have reported ESCRT-III spirals that can grow to several hundred nm in radius (*18, 21*), without deforming the membrane on their own (*1, 22*).

ESCRT-III filaments have also been observed in a variety of 3D shapes, such as helices and cones (*1, 16, 19, 22–25*), indicating that ESCRT-III filaments can assume alternative target geometries. To account for this, we extended our model to include 3D filaments. We then allowed filaments to switch between two well-defined categories of geometrical states. In the first category, the target geometry is a flat ring, leading to the formation of spirals when bound to a membrane. In the second, the filament takes on a 3D helical shape, in which its membrane attachment site has rotated towards the outside of the helix (*23*). This is accomplished by twisting the target ring geometry by an angle τ (Fig. 2a). We suggest that this internal filament rotation, which has not been taken into account in previous models (*14–16*), drives membrane deformation. When a planar spiral-shaped filament is placed on a flat membrane and the target geometry is switched throughout the filament to the ”twisted” state, we observe that the relaxation of the filament is accompanied by a clear buckle in the membrane. This deformation develops away from the cytoplasm, and grows in time to a fixed depth (Fig. 2b, Video 2).

This works as follows. The membrane deformation is initiated by the filament twist which transforms the filament-membrane attraction site from a 2D plane to a 3D conical surface with aperture $\theta = 90^\circ - \tau$. This initiates an out-of-plane membrane deformation, which frees the filament from being trapped in a 2D plane, allowing the filament arms to move in 3D and relax closer to their desired radius R. While doing so, the outer filament arms push the inner arms down into the buckle, deepening the deformation. Because this is achieved via volume exclusion, tension in the filament only makes an indirect contribution to membrane deformation by encouraging the filament to enter the buckle (see SI and Video 4 and 5 for a control experiment). The resulting filament assumes a tightly-coiled helical geometry, even though the filament does not possess a pitch in its target geometry.

While helical filaments will attempt to relax into a state in which neighbouring rings are stacked and tilted by τ, the wrapping of membrane about each ring of the spiral in the twisted state is not energetically favourable. The trade-off deformation is therefore a cone. Only for filament twists of $\tau = 90^\circ$ do we observe tubule formation (Fig. 3a).

We found the filament twist angle has the most impact on the shape of the deformation by determining its form and direction. This is shown in Fig. 3b, where the depth and the sign of the deformation depend on the twist angle and the radius of the twisted state, starting from an identical initial, flat state. Strikingly, a single model parameter generates a large variety of observed states ranging from flat spirals, to conical helices of varying aperture and even tubules in both directions.

The depth of the deformation is also influenced by the preferred filament radius (Fig. 3b) and filament rigidity (Fig. 3c). Since the filaments in our simulations are of constant lengths, filaments of large preferred radii will result in shorter helices and will yield shallower deformations. The persistence length functions here as a measure of the amount of inner tension that the filament possesses. Naturally, filaments with small persistent lengths do not have a strong drive to achieve their target geometry, and cannot deform the membrane (Fig. 3c). For increasing persistence lengths, deeper buckles develop, and their shape changes from conical towards tubular. The internal filament energy now dominates over the elastic energy to bend the membrane, and a tubular deformation that accommodates the preferred filament radius is formed. Finally, to test the possible role of the helical pitch, which is not implemented in our model, we also repeated our simulations with introducing an explicit helical pitch in the twisted state (see SI). Interestingly, we found that it does not influence the resulting deformations and that the filament always remains in a tightly-coiled helix state when deforming the membrane (Fig. S4).

The model also provides a simple and intuitive explanation for the origin of the symmetry breaking in the membrane deformation. The buckling direction is determined by the sign of the twist angle τ, i.e. by 3D chirality in the filament. We should therefore be able to reverse the buckle direction simply by reversing the filament twist. As can be seen in Fig. 2c and 3b by moving membrane-binding sites to the inside of the filament, buckles can be induced in the opposite direction, towards the cytoplasm (Video 3). In line with this possibility, Cullough et al. reported the formation of both upward and downward buckles of ESCRT-III filaments, depending on the filament composition (*3*). Hence it is possible that ESCRT-III filaments could induce different geometries depending on whether a spiral changes into a twisted helix or into an inverted twisted helix.

Interestingly, in our model there is a bias in the system that leads to a preference for downward buckles (as can be seen in Fig. 3b). Simulations for large negative twist angles ($\tau = -80^{\circ}$ to -90°) do not show any deformation, an anomaly that is not mirrored for positive twist angles. The reason for this bias in the energy landscape is that, for an upward buckle to form, the membrane must adhere to the filament from “the inside” and must adopt a larger curvature than a downward membrane deformation caused by the same amount of the filament twist, rendering upward deformations more costly. In the case of downward deformations, the membrane envelops the filament from the outside, resulting in a smaller curvature, reducing the amount of energy required to deform the membrane. These observations may explain why cytosolic ESCRT-III filaments preferentially deform and cut membranes away from the cytoplasm.

To explore whether transitions in filament geometry can also drive scission, we introduced a simple generic cargo into the model. This cargo is allowed to weakly adhere to the membrane (see SI for details) so that it remains adsorbed and partially wrapped but without undergoing spontaneous budding. We then polymerise a flat ESCRT-III spiral around the cargo. This models the way the ESCRT system is thought to corral cargo in cells (*26*). Under these conditions, a switch in filament geometry, induced by a transition to a positively twisted state, initiates a conical membrane deformation, which traps the cargo at its centre underneath the ESCRT-III helix, as shown in Fig. 4. In this configuration, the filament stabilises the energetically-costly membrane neck. If the filament geometry reverts back to a flat state, this destabilises the neck and causes membrane scission, releasing a membrane bud that carries the cargo particle, while the filament retracts back to the cytoplasm. Thus, transitions between distinct geometrical states can drive ESCRT-III-mediated membrane scission to mimic the role of ESCRT-III in the formation of vesicles.

This minimal coarse-grained model of ESCRT-III filaments in contact with lipid membranes captures many of the experimentally observed behaviours of this versatile membrane apparatus, including different filament morphologies, diverse membrane deformations, scission, as well as cargo-loaded membrane budding and ESCRT recycling (*27*). The key ingredient of the model is the transition of the filament between two different geometrical states – a flat one, where the membrane-binding sites of the filament lie on a flat plane inhibiting membrane deformation, and a twisted one, where the membrane-binding sites shift into a 3D surface.

How might the different geometrical states be achieved in the context of ESCRTIII functions *in vivo*? We suggest that the presence of different members of the ESCRT-III family of proteins in copolymers (*3, 4, 23, 28*), may control the overall geometrical state of the filament. Thus, changes in the composition of the filament induced through the action of the Vps-4 ATPase as it induces filament depolymerization/turnover, as has been widely suggested (*22, 29*), would change the internal structure of the filament toward a different target geometry, leading to membrane deformation and scission. This fits with the experimental evidence that binding partners of ESCRT-III can change filament structure (*3, 30–32*) and transform flat spiral filaments into helices (*1, 22*). The large variety of ESCRT-III binding partners enables the filament to move across a whole field of target geometries depending on the copolymer composition, thereby facilitating diverse ESCRT functions on very different scales and topologies. We expect that similar geometrical transitions between or even within states may also enable ESCRT-III filaments to function in membrane healing and cell division. Local rather than global transitions can even lead to mixed geometry filaments that are flat on the outside and helical in the centre (*3*).

In summary, this general physical model captures a novel non-equilibrium mechanism of membrane remodelling by elastic filaments as they undergo a global change in geometry. In our simulations the energy required to drive these transitions is effectively supplied into the system by altering the filament geometry, which mimics the changes in the filament chemical composition. This coupling between the chemical composition and filament geometry produces mechanical work with which membranes can be deformed and cut. Beyond its contribution to the understanding of the ESCRT-III apparatus and membrane remodelling, our model also opens a range of possibilities for studies of membrane physics during energy-driven processes. Our results also suggest a novel way of controlling membrane remodelling in synthetic systems, applicable for instance to membrane-deformation by self-assembled DNA origami structures (*33*), where geometrical transition of the systems should be relatively straightforward to control.

References

1. W. M. Henne, N. J. Buchkovich, Y. Zhao, S. D. Emr, *Cell* **151**, 356 (2012).
2. A. G. Cashikar, *et al.*, *Elife* **3**, e02184 (2014).
3. J. McCullough, *et al.*, *Science (New York, N.Y.)* **350**, 1548 (2015).
4. G. Effantin, *et al.*, *Cellular microbiology* **15**, 213 (2013).
5. J. G. Carlton, J. Martin-Serrano, *Science* **316**, 1908 (2007).
6. E. Morita, *et al.*, *The EMBO Journal* **26**, 4215 (2007).
7. R. L. Williams, S. Urbé, *Nature Reviews Molecular Cell Biology* **8**, 355 EP (2007).

8. T. Wollert, C. Wunder, J. Lippincott-Schwartz, J. H. Hurley, *Nature* **458**, 172 (2009).
9. M. A. Y. Adell, *et al.*, *The Journal of Cell Biology* **205**, 33 (2014).
10. U. K. von Schwedler, *et al.*, *Cell* **114**, 701 (2003).
11. P. D. Bieniasz, *Virology* **344**, 55 (2006). Virology 50th Anniversary Issue.
12. A. J. Jimenez, *et al.*, *Science* **343**, 1247136 (2014).
13. C. L. Stoten, J. G. Carlton, *Seminars in cell & developmental biology* (Elsevier, 2018), vol. 74, pp. 50–65.
14. M. Lenz, D. J. G. Crow, J.-F. m. c. Joanny, *Phys. Rev. Lett.* **103**, 038101 (2009).
15. G. Fabrikant, *et al.*, *PLoS computational biology* **5**, e1000575 (2009).
16. N. Chiaruttini, A. Roux, *Current Opinion in Cell Biology* **47**, 126 (2017). Cell Organelles.
17. J. Agudo-Canalejo, R. Lipowsky, *PLoS computational biology* **14**, e1006422 (2018).
18. N. Chiaruttini, *et al.*, *Cell* **163**, 866 (2015).
19. R. Pires, *et al.*, *Structure* **17**, 843 (2009).
20. S. Ghazi-Tabatabai, *et al.*, *Structure* **16**, 1345 (2008).
21. Q.-T. Shen, *et al.*, *The Journal of Cell Biology* **206**, 763 (2014).
22. P. I. Hanson, R. Roth, Y. Lin, J. E. Heuser, *The Journal of Cell Biology* **180**, 389 (2008).
23. S. Lata, *et al.*, *Science (New York, N.Y.)* **321**, 1354 (2008).
24. M. J. Dobro, *et al.*, *Molecular biology of the cell* **24**, 2319 (2013).

25. I. Goliand, *et al.*, *Cell reports* **24**, 1756 (2018).

26. D. Teis, S. Saksena, B. L. Judson, S. D. Emr, *The EMBO journal* **29**, 871 (2010).

27. J. Schöneberg, I.-H. Lee, J. H. Iwasa, J. H. Hurley, *Nature reviews Molecular cell biology* **18**, 5 (2017).

28. W. M. Henne, H. Stenmark, S. D. Emr, *Cold Spring Harbor Perspectives in Biology* **5**, a016766 (2013).

29. J. Schoeneberg, *et al.*, *bioRxiv* p. 262170 (2018).

30. M. Babst, D. J. Katzmann, E. J. Estepa-Sabal, T. Meerloo, S. D. Emr, *Developmental Cell* **3**, 271 (2002).

31. D. Teis, S. Saksena, S. D. Emr, *Developmental Cell* **15**, 578 (2008).

32. Y. Avalos-Padilla, *et al.*, *Frontiers in Cellular and Infection Microbiology* **8**, 53 (2018).

33. H. G. Franquelim, A. Khmelinskaia, J.-P. Sobczak, H. Dietz, P. Schwille, *Nature communications* **9**, 811 (2018).

Acknowledgments

We thank Jeremy Carlton, Mike Staddon, Geraint Harker, and members of the Wellcome Trust Consortium ”Archaeal Origins of Eukaryotic Cell Organisation” for fruitful conversations. We thank Peter Wirnsberger and Tine Curk for discussions about the membrane model implementation. We acknowledge funding from BBSRC LIDo DTP (L.H.K.), the Wellcome Trust (B.B.), and Royal Society (A.Š.).

Supplementary materials

Supplementary Information.

Figures S1 to S4.

Videos V1 to V6.

References *(1-6)*.

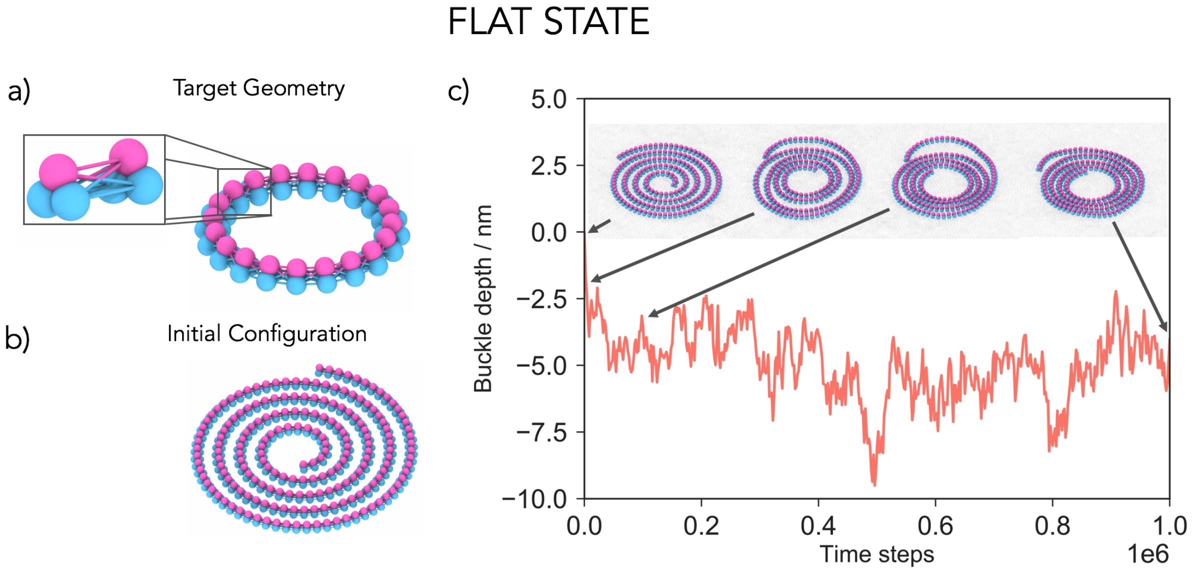

Figure 1: **Model development.** **a)** Filaments are built out of interconnected three-beaded units. The target geometry of the filament is a flat ring whose radius is determined by the rest lengths of bonds between the triplet units. The inset highlights two neighbouring units connected by 9 bonds to preserve the spiral chirality. The blue beads of the triplet are attracted to the membrane. **b)** If the filament is longer than the circumference of the target ring, it will acquire a geometry of a spiral with tense bonds, which is our initial configuration of the system. **c)** Placing a flat spiral on the membrane does not lead to a significant membrane deformation. The filament density increases, but its membrane-attracted face remains trapped in the same 2D plane. A shallow buckle that develops around -5 nm is due to the membrane enveloping the filament to maximize their contact surface. The arrows highlight simulation snapshots at specific time steps. The radius of the target geometry is $R = 20.4$ nm and the persistence length of the filament $l_\mathrm{p} = 1.8 \cdot 10^3$ nm.

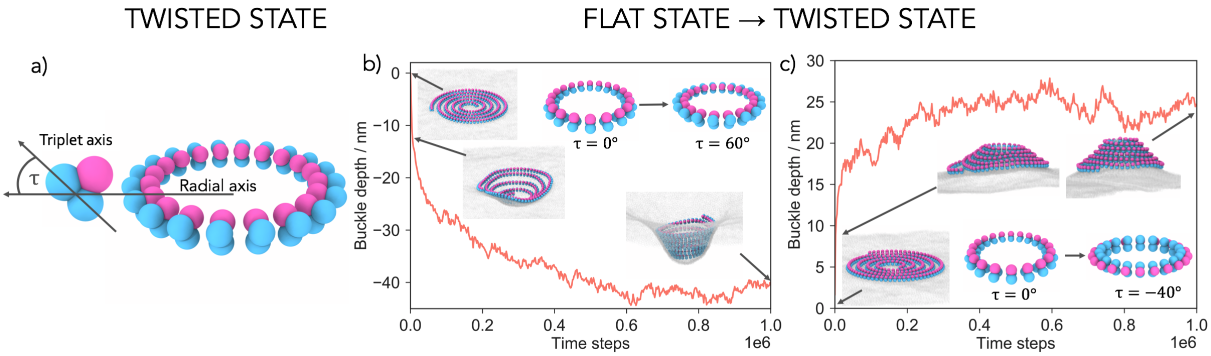

Figure 2: **Transition between filament geometries creates membrane deformation. a)** The Twisted state is defined by a twist angle τ, which is the angle between the radial axis and the triplet subunit axis. **b)** Switching from the flat to twisted ring ($\tau = 60^\circ$, depicted in the inset) creates downward membrane deformations, away from the cytoplasm. The curve shows the depth of the deformation over time ($R = 15.3$ nm and $l_\mathrm{p} = 1.8 \cdot 10^3$ nm). **c)** The direction of the deformation can be reversed by twisting the filament outwards, rather than inwards. The new target geometry is now a ring with $\tau = -40^\circ$, $R = 11.5$ nm, and $l_\mathrm{p} = 1.8 \cdot 10^3$ nm. The underlying curve shows the height of the developing deformation over time.

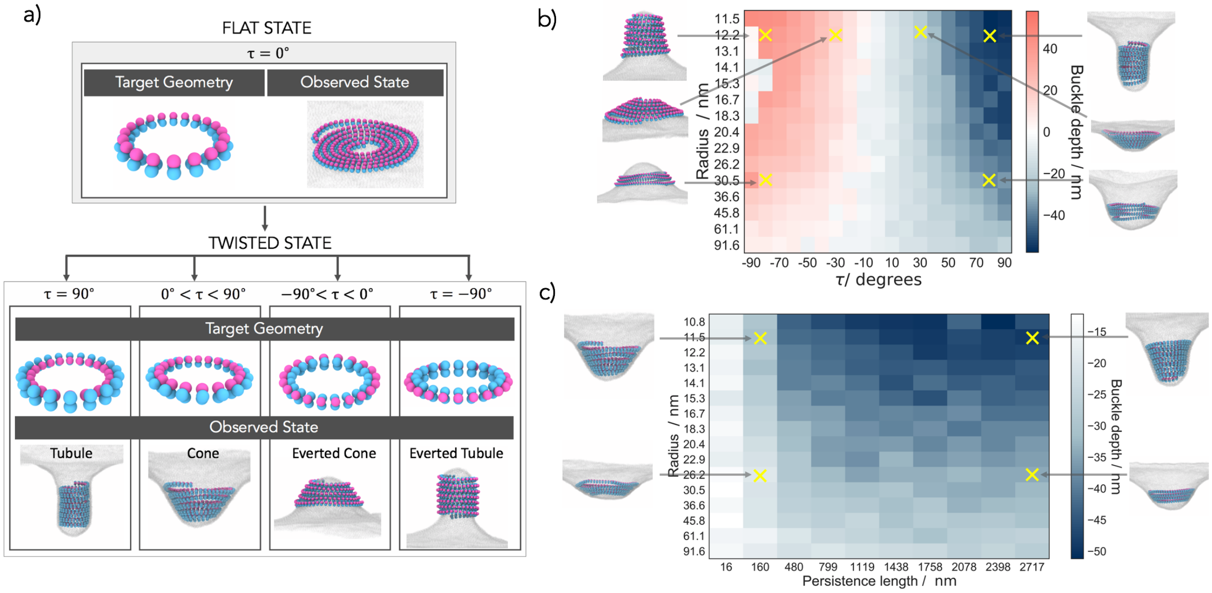

Figure 3: **The filament twist determines the shape and sign of the membrane deformation.** An overview of the two-state model, providing examples for different outcomes. In the flat state the target geometry is a planar ring with the membrane attraction sites facing downwards ($\tau = 0°$) and the filament is observed as a flat spiral. By twisting the target geometry ring we enter the twisted state tubules develop for $\tau = 90°$, cones for $0° < \tau < 90°$, everted cones for $\tau < 0°$, and everted tubules for $\tau = -90°$. **b)** The buckle depth dependence on the target radius R and twist angle τ of the twisted state. Each simulation started off with the same initial spiral in the flat state with persistence length $l_\mathrm{p} = 1.8 \cdot 10^3$ nm. **c)** The buckle depth dependence on the target radius R and the persistence length l_p of the twisted state ($\tau = 60°$) . Each simulation started off with the same initial spiral in flat state. The insets show snapshots of the representative cases.

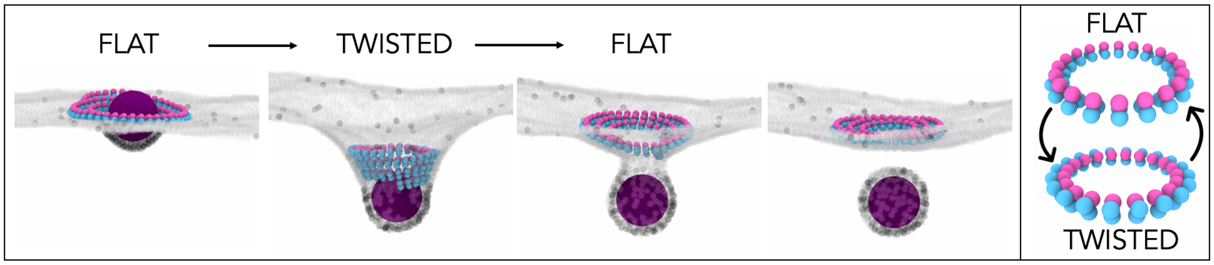

Figure 4: **Repetitive filament transitions can sever membranes.** Left panel: A filament is polymerised around a cargo (magenta sphere) that binds to the dark receptors in the membrane but cannot bud off on its own. Switching from a flat ($R = 12.2$ nm, $\tau = 0°$) to a twisted State ($R = 12.2$ nm, $\tau = 60°$) causes the membrane deformation. Switching back from the twisted to the flat state causes cargo budding where the filament is released back to the cytoplasm. Right panel: Target geometries of the flat and twisted states.